John von Neumann Institute for Computing

Generation of Plate-Tectonic Behavior and a New Viscosity Profile of the Earth's Mantle

Uwe Walzer, Roland Hendel, John Baumgardner

published in

NIC Symposium 2004, Proceedings,
Dietrich Wolf, Gernot Münster, Manfred Kremer (Editors),
John von Neumann Institute for Computing, Jülich,
NIC Series, Vol. **20**, ISBN 3-00-012372-5, pp. 419-428, 2003.

http://www.fz-juelich.de/nic-series/volume20

Generation of Plate-Tectonic Behavior and a New Viscosity Profile of the Earth's Mantle

Uwe Walzer[1], **Roland Hendel**[1], **and John Baumgardner**[2]

[1] Institut für Geowissenschaften, Friedrich-Schiller-Universität
Burgweg 11, 07749 Jena, Germany
E-mail: {walzer, hdl}@geo.uni-jena.de

[2] Los Alamos National Laboratory, MS B216 T-3, Los Alamos, NM 87545, USA
E-mail: baumgardner@lanl.gov

This paper reports a series of compressible spherical-shell convection calculations with a new viscosity profile, called *eta3*, that is derived from PREM and mineral physics. The viscosity profile displays not only a high-viscosity lithosphere and a *viscosity hill* in the *central* region of the *lower mantle* of the Earth but also a prominent *high-viscosity transition layer* inferred to arise from a high garnet content. Moreover, there is not only the usual asthenosphere but also a *second low-viscosity zone just below the 660-km* discontinuity. We introduced a viscoplastic yield stress and obtained *plate-like movements* near the surface. A variation of the parameters revealed a Rayleigh-number–yield-stress area where the plate-tectonic character of the solution is stable and pronounced. Runs with *eta3* but without any yield stress show networks of reticularly connected very thin sheet-like downwellings but, of course, no plates. For calculations with *eta3* plus yield stress, the distributions of the downwellings are more Earth-like.

1 Introduction

There are some mantle-convection problems that are unresolved. For some other problems of that kind, different authors proposed contradictory solutions. If simply viscous rheology with temperature dependence of the viscosity is supposed then three types of solution are possible (Solomatov[31]) but no type of them shows piecewise plate-like behavior like the real Earth. Christensen and Harder[8] proved that no plate-like pattern emerges with a Newtonian rheology. So, a *first* problem is the self-consistent generation of plates near the surface from an assumed rheology. It is well-known that some oceanic lithospheric plates are obliquely subducted into the mantle. Seismic tomography revealed that a lot of slabs penetrate the 660-km discontinuity and arrive at considerable depths but not in each case at the core-mantle boundary (CMB) (Grand et al.[13]; van der Hilst et al.[39]; Ritsema and van Heijst[29]). A *second* problem is that most convection calculations show considerably too broad downwellings in the upper mantle (UM), too broad in comparison with observation. The real cold downwelling slabs are rather thin in the UM. In an equal-area projection of a fixed UM depth, the temperature distribution should show loosely connected, very thin cold stripes with a similar distribution as modern earthquake foci but not a narrow-meshed network of thin lines or even broad downwellings. A *third* problem is that many thermal-convection calculations take into account only the temperature dependence of the viscosity so that the radial variation of viscosity is mainly confined to the two thermal boundary layers. However, the pressure dependence of the concentrations of Schottky and Frenkel defects and of the dislocations produces large additional radial changes of the effective viscosity of the mantle. Moreover, the proposed viscosity profiles of different authors (King and Masters[19]; Panasyuk and Hager[26]; Forte and Mitrovica[10]; Kaufmann

and Lambeck[18]) differ considerably from each other. Therefore it seems suitable to compare thermal-convection runs with very different viscosity profiles. A *fourth* problem is the long-term coupling between plates and mantle convection. Bunge and Richards[6] superimposed a given velocity field to study the circulation whereas Gable et al.[11] and Monnereau and Quéré[24] presented models with plates overlying a mantle with viscosity stratification. The plate motion balances the torque of stresses generated by mantle convection. These models form a contrast to models with a self-consistent generation of plates. The water-rich Earth has a plate-tectonic regime whereas the now water-poor planets Mars and Venus have a hot-spot regime and a stagnant lid. Therefore, models with a self-lubricating rheology (Bercovici[3]), void production and ingestion of volatiles (Bercovici[4]) and a two-phase model for compaction and damage (Bercovici et al.[5]; Ricard et al.[27]) seem to be very promising. The approach of Trompert and Hansen[38] is interesting, too. Another self-consistent generation of plates is feasible by pseudoplastic yielding (Tackley[36]) or by strain weakening. (Tackley[37]). Also Richards et al.[28] investigated the plate generation by yield stress.

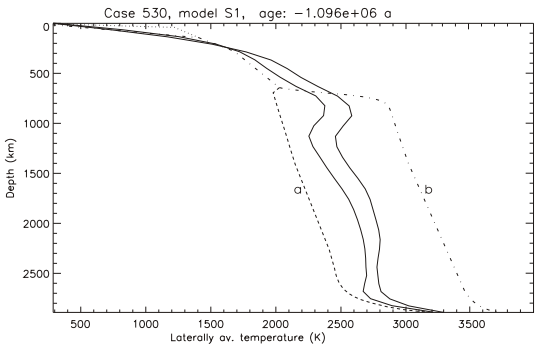

Figure 1. Possible present-day geotherms. See text.

2 Model

The model is based on the numerical solution of the balance equations of energy, momentum and mass. The solid-state convection of the Earth's mantle is represented by an infinite Prandtl number fluid in a compressible spherical shell heated mainly from within by the radioactive elements of the primordial mantle. The concentrations are taken from McCulloch and Bennett[23]. A general derivation of such kind of equations is given by Narasimhan[25] and Schubert et al.[30]. The present model differs from the model S1 of us mainly by three issues:

a) S1 tested the hypothesis that, at the CMB, not the temperature, T_c, but the heat flow, q_c is a constant *with respect to time* . This assumption was based on results of Stevenson et al.[35], Stacey[32](Chapter 6.7.5) and Schubert et al.[30], pp. 607-609. In the present paper, however, we abandon this assumption: Here, T_c *and* q_c are temporal functions, but T_c is laterally constant. As other researchers (Steinbach et al.[33]; Steinbach and Yuen[34]; Honda and Iwase[14]) have done when implementing cooling core-mantle evolution models, we adjust T_c after each time step according the heat flow through the CMB.

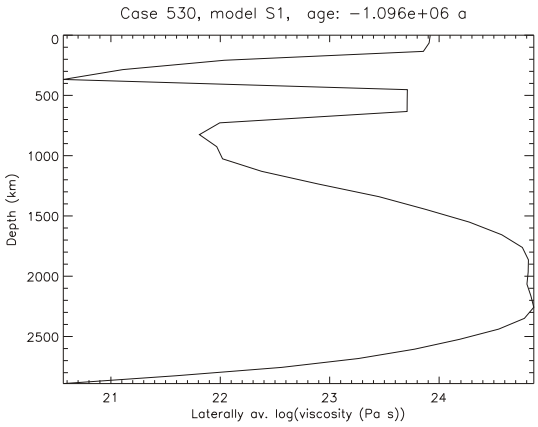

Figure 2. Present-day viscosity profile of run 530.

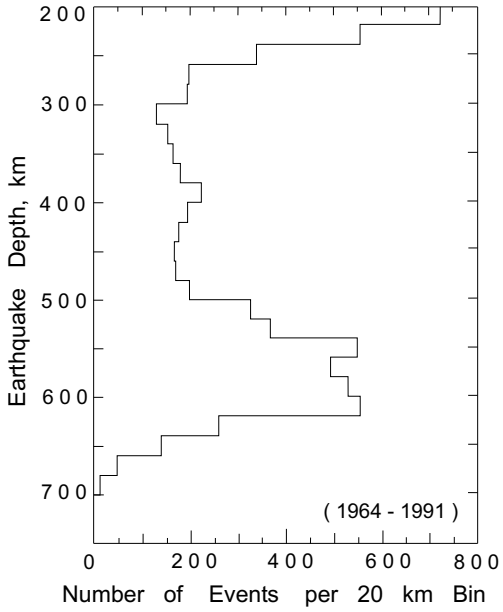

Figure 3. Frequency distribution of earthquakes as a function of depth according to Kirby et al.[20].

b) Based on results of Karato and Li[15], Karato and Wu[17] and Li et al.[21], we assume a Newtonian creep for the mantle. In this paper, however, we supplement this assumption by an additional viscoplastic stress, σ_y, for the uppermost 285 km. The yielding is implemented by an effective viscosity, η_{eff}, where

$$\eta_{eff} = \min[\eta(P,T), \frac{\sigma_y}{2\dot{\varepsilon}}]. \quad (1)$$

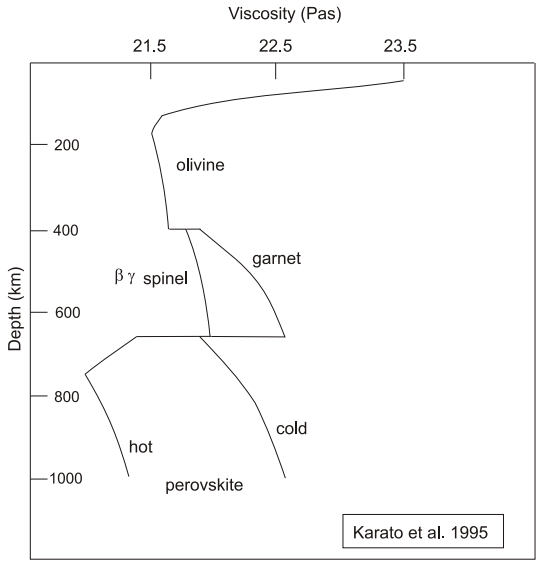

Figure 4. The viscosity profile for cold slabs and hot plumes according to Karato et al.[16].

In this formula, $\dot{\varepsilon}$ is the second invariant of the strain-rate tensor, P is the pressure and T the temperature.
c) In $this$ paper, a viscosity profile is deduced that depends only slightly on mineralogical assumptions. The Birch-Murnaghan equation was employed to derive the Grüneisen parameter and other physical quantities as a function of depth from observational values provided by the seismic model PREM (Dziewonski and Anderson[9]). We computed the melting temperature, T_m, and a new mantle viscosity profile, called *eta3*, using the Grüneisen parameter, Lindemann's law and some solid-state physics. We use for the viscosity, η, the formula

$$\eta(r,\theta,\phi,t) = 10^{r_n} \cdot \eta_3(r) \cdot \exp\left[c_t \cdot T_m(r) \cdot \left(\frac{1}{T(r,\theta,\phi,t)} - \frac{1}{T_{av}(r,t)}\right)\right], \quad (2)$$

where T_{av} is the laterally averaged temperature, r the radius, θ the colatitude, ϕ the longitude, t the time, c_t a constant, r_n the viscosity-level parameter.

3 Results

Before we show the global distribution of the different types of solution of the model by variation of the parameters, we present two types of solution by two specific runs: Case 530 is a run without plates near the surface, but else it is rather mantle-like. Run 574 shows plate-like movements near the surface and else it is also mantle-like. Fig. 1 shows the present-day laterally averaged temperature (right solid line) obtained by run 530 using the directly computed melting temperature. If we repeat this run with a melting temperature where, in the upper 15 GPa of the mantle, our theoretical T_m-curve is replaced by experimental values of Zhang and Herzberg[42] (See also Zerr at al.[41]), then the left solid

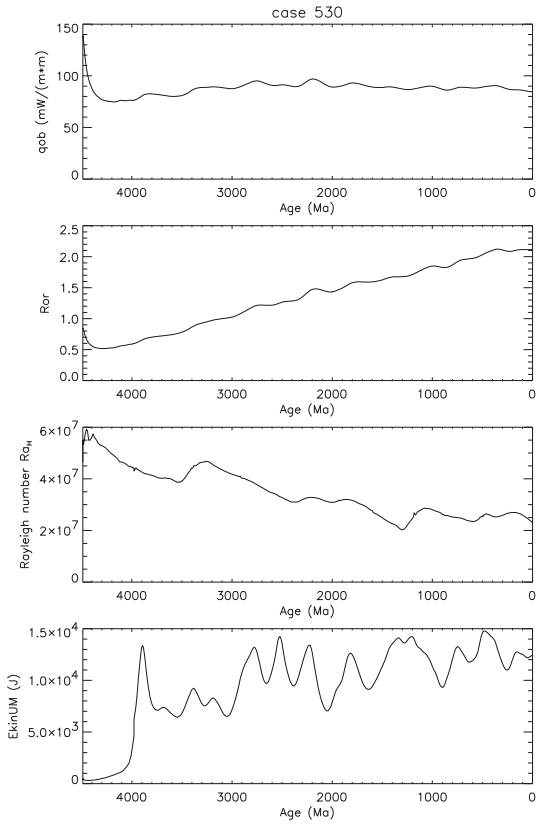

Figure 5. The evolution of the quantities *qob*, *Ror*, Ra_H and *EkinUM* . See text.

line stands for T_{av}. In this case, the surface heat outflow is larger. Run 530 is for $r_n = 0$ and $\sigma_y = 180$ *MPa* . For comparison, the range of possible mantle geotherm according to Schubert et al.[30] is shown. Label a and b denote geotherms of whole-mantle and partially layered convection, respectively. The dotted line near the surface corresponds to a ridge geotherm. Fig. 2 presents the laterally averaged viscosity of run 530 for the geological present. It reflects the essential features of *eta3*. For lack of space, it is not possible to deduce *eta3* in this paper. In the following, only some hints are given to make the high-viscosity transition layer plausible. We adopt the usual assumption that the subducting slab of the real Earth is cooler than the surrounding. Therefore, the downgoing oceanic lithosphere has a higher viscosity than the surrounding. If the slab penetrates a highly viscous layer on its way to the depth then shear stress should be collected that will be released in earthquakes in the short-period range. This is indeed observed (See Fig. 3). Based on experimental mineral physics, already Karato et al.[16] concluded that the transition layer has a higher viscosity than the neighboring layers (See Fig. 4). The segregation of the early Earth into a primordial silicate mantle and an iron core was finished at an age of 4490 Ma or earlier. Therefore, our dynamical-evolution models of the Earth's mantle start at this age. The first panel of Fig. 5 shows the laterally averaged heat flow at the Earth's surface,

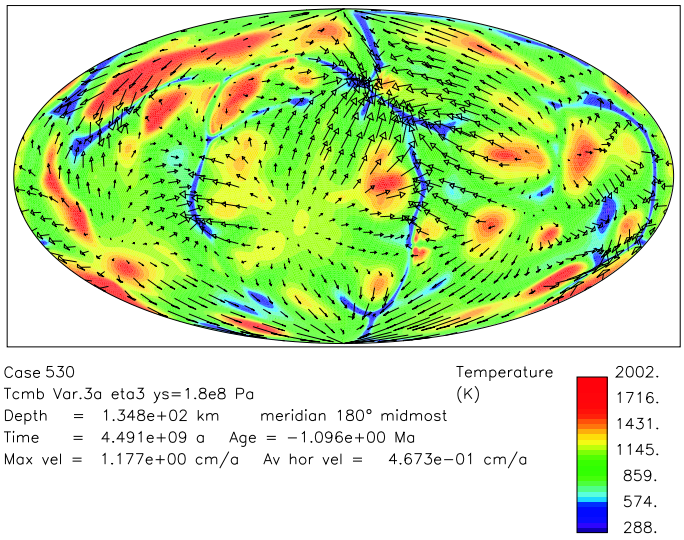

Figure 6. Equal-area plot of run 530 with $\sigma_y = 180$ *MPa* in 134.8 km depth. This case is not plate like (See text).

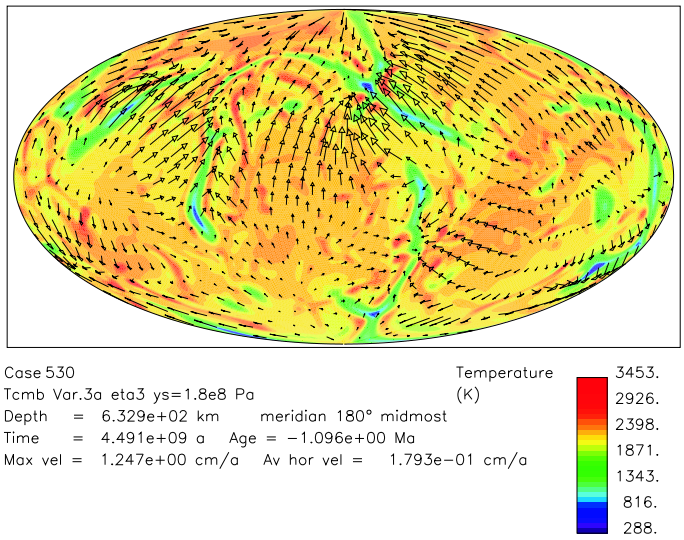

Figure 7. Equal-area plot of run 530 in 632.8 km depth (See text).

qob, as a function of the time in the past. The present-day value is very realistic. The second panel represents the reciprocal Urey number, Ror. The temporal average of Ror is called $\overline{Ror}$. The quantity $\overline{Ror}$ of run 530 is 1.339. Schubert et al.[30] estimate the possible interval for Earth and Venus: $1.25 < \overline{Ror} < 1.67$. The third panel of Fig. 5 presents the

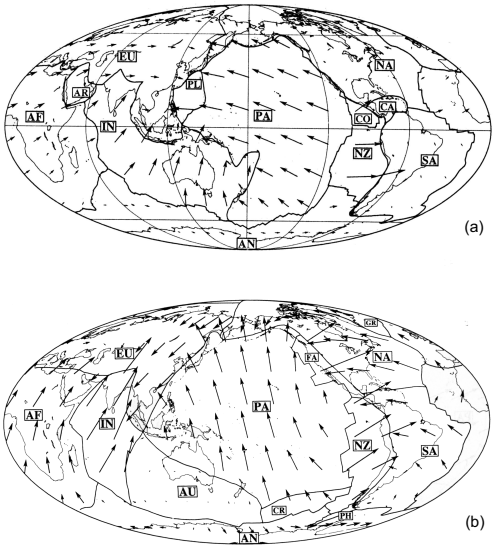

Figure 8. Observed lithospheric plates and their lateral velocities relative to the high-viscosity layer of the lower mantle. (a)0-10 Ma ago, (b) 43-48 Ma ago. According to Lithgow-Bertelloni and Richards[22].

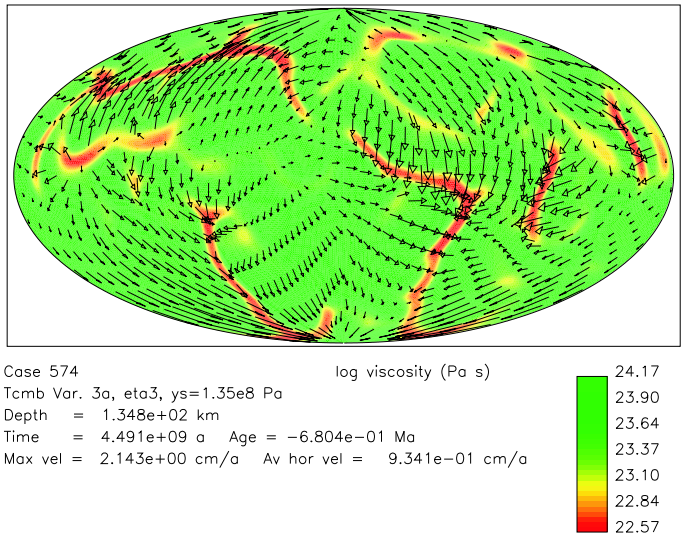

Figure 9. Equal-area projection of run 574 with $\sigma_y = 135$ *MPa* for the geological present. Arrows denote the creeping velocity, colors stand for the viscosity.

evolution of the Rayleigh number, Ra_H, that is given by

$$Ra_H = \left\langle \frac{\rho \alpha g h^3}{\kappa \eta_{al}} \cdot \frac{(\mathcal{Q} h + q_c)\, h}{k} \right\rangle , \tag{3}$$

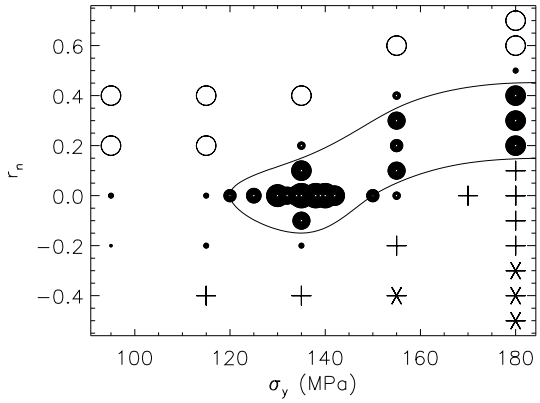

Figure 10. The character of the solutions as a function of the viscosity-level parameter, r_n, and the yield stress, σ_y. Further explanations see text.

where ρ is the density, α thermal expansion coefficient, g gravity acceleration, h depth of the layer, Q is the heat generation rate per unit volume, q_c the heat flow at the CMB, κ thermal diffusivity, k thermal conductivety. The quantity η_{al} is given by

$$\log \eta_{al} = \langle \log \eta \rangle \, . \tag{4}$$

The bracket $\langle\rangle$ denotes a volumetric average. The fourth panel shows the kinetic energy of UM convection. This is perhaps a measure of the orogenetic activity. Of course, the position of the maxima is not very stable from run to run whereas the evolution of qob, Ror and Ra_H do not vary very much for investigated parameter range (See Fig. 10). Fig. 6 presents the temperature distribution (colors) and the creeping velocities (arrows) for the geological present in a depth of 134.8 km. For plate-like cases, the velocity is plate-like in this depth, yet. But run 530 does not show plate tectonics. However, the downwellings are tabular-shaped. Fig. 7 shows the continuation in 632.9 km depth: The slab-like features cross the high-viscosity transition layer. They are only partly joined with each other as the slabs of the real Earth. Contrary to the real subducting slabs of the Earth, the downwellings of the model descent perpendicularly. This is not amazing since the model contains no continents up to now. Contrary to other models, Fig. 6 shows already an Earth-like distribution of the thin downwellings. The T_l^{rms}-spectrum (not shown) is also Earth-like. Panel (a) of Fig. 8 presents the observed creeping velocities at the present-day surface of the solid Earth, panel (b) shows this observed movements 43-48 Ma ago. This plate like observations are in contradiction to Fig. 6 of run 530. Therefore, we repeat this run changing only one parameter: Case 574 was calculated with a yield stress, σ_y, of 135 MPa. Fig 9 reveals piecewise plate-like movements in 134.8 km depth. The distribution of the velocities at the surface is nearly the same. Colors signify the viscosity. Subduction zones and spreading zones have reduced viscosity. In corresponding equal-area plots of greater depth, cold narrow stripes are situated perpendicularly beneath the subduction zones of Fig. 9. Such a type of solution is characterized by little black disks with a white center in Fig. 10 where the results of the variation of the parameters are shown. The viscosity-level parameter, r_n, is a monotonous function of a temporally averaged Rayleigh number. Fig. 10 shows three

other types of solution, yet: Plus signs denote runs without plates but with thin elongated slab-like downwellings. Run 530 belongs to that type. Asterisks represent runs without surface plates and without slab-like downwellings. White circles stand for runs without plates near the surface that have a wide-meshed network of broad downwellings. The conclusions can be found in the abstract.

4 Numerical Method and Implementation

The solutions of the system of differential equations of convection in a compressional spherical shell are obtained using a three-dimensional finite-element discretization, a fast multigrid solver and the second-order Runge-Kutta procedure. The mesh is generated by projection of a regular icosahedron onto a sphere to divide the spherical surface into twenty spherical triangles or ten spherical diamonds. A dyadic mesh refinement procedure connects the midpoints of each side of a triangle with a great circle such that each triangle is subdivided into four smaller triangles. Successive grid refinements generate an almost uniform triangular discretization of the spherical surface of the desired resolution. Corresponding mesh points of spherical surfaces at different depths are connected by radial lines. The radial distribution of the different spherical-surface triangular networks is so that the volumes of the cells are nearly equal. More details are given by Baumgardner[1,2], Bunge et al.[7] and Yang[40]. For the multitude of runs we needed for our parameter study, we employed a mesh with 1351746 nodes. Some runs were made with 10649730 nodes to check the convergence of the lower resolution runs. The result is that the laterally averaged heat flow, the ratio of heat outflow to radiogenic heat production, the Rayleigh number, and the Nusselt number as functions of the time show hardly any discernable differences (< 0.5 %). Calculations were performed on 128 processors of a Cray T3E. The code was benchmarked for constant viscosity convection by Bunge et al.[7] with numerical results of Glatzmaier[12] for Nusselt numbers, peak temperatures, and peak velocities. A good agreement (≤ 1.5 %) was found.

Acknowledgments

This research was supported by the John von Neumann Institute for Computing, Forschungszentrum Jülich, and by the Höchstleistungsrechenzentrum Stuttgart through the supply of computing time.

References

1. Baumgardner, J.R., 1983. Thesis, Univ. of California, Los Angeles.
2. Baumgardner, J.R., 1985. J. Stat. Phys. 39 (5-6), 501-511.
3. Bercovici, D., 1996. Earth Planet. Sci. Lett. 144, 41-51.
4. Bercovici, D., 1998. Earth Planet. Sci. Lett. 154, 139-151.
5. Bercovici, D., Ricard, Y., Schubert, G., 2001. J. Geophys. Res. 106, no. B5, 8887-8906.
6. Bunge, H.P., Richards, M.A., 1996. Geophys. Res. Lett. 23, 2987-2990.

7. Bunge, H.-P., Richards, M.A., Baumgardner, J.R., 1997. J. Geophys. Res. 102, 11991-12007.
8. Christensen, U., Harder, U., 1991. Geophys. J. Int.. 104, 213-226.
9. Dziewonski, A.M., Anderson, D.L., 1981. Phys. Earth Planet. Inter. 25, 297-356.
10. Forte, A.M., Mitrovica, J.X., 2001. Nature 410, 1049-1056.
11. Gable, C.W., O' Connell, R.J., Travis, B.J., 1991. J. Geophys. Res. 96, 8391-8405.
12. Glatzmaier, G.A., 1988. Geophys. Astrophys. Fluid Dyn. 43, 223-264.
13. Grand, S.P., van der Hilst, R.D., Widiyantoro, S., 1997. GSA Today 7, 1-7.
14. Honda, S., Iwase, Y., 1996. Earth Planet. Sci. Lett. 139, 133-145.
15. Karato, S.-i., Li, P., 1992. Science 255, 1238-1240.
16. Karato, S.-i., Wang, Z., Liu, B., Fujino, K., 1995, Earth Planet. Sci. Lett. 130, 13-30.
17. Karato, S.-i. Wu, P., 1993. Science 260, 771-778.
18. Kaufmann, G., Lambeck, K., 2002. J. Geophys. Res. 107, no. B11, 2280, doi: 10.1029/2001JB000941.
19. King, S.D., Masters, G., 1992. Geophys. Res. Lett. 19, 1551-1554.
20. Kirby, S.H., Stein, S., Okal, E.A., Rubie,D.C., 1996. Rev. Geophys. 34, 261-306.
21. Li, P., Karato, S.-i., Wang, Z., 1996. Phys. Earth Planet. Inter. 95, 19-36.
22. Lithgow-Bertelloni, C., Richards, M.A., 1998. Rev. Geophysics 36, 27-78.
23. McCulloch, M.T., Bennett, V.C., 1994. Geochim. Cosmochim. Acta 58, 4717-4738.
24. Monnereau, M., Quéré, S., 2001. Earth Planet. Sci Lett. 184, 575-587.
25. Narasimhan, M.N.L., 1993. Wiley, New York etc, 567 pp.
26. Panasyuk, S.V., Hager, B.H., 2000. Geophys. J. Int. 143, 821-836.
27. Ricard, Y., Bercovici, D., Schubert, G., 2001. J. Geophys. Res. 106, 8907-8924.
28. Richards, M.A., Yang, W.-S., Baumgardner, J.R., Bunge, H.-P., 2001. Geochemistry, Geophysics, Geosystems vol. 2, paper no.2000GC000115.
29. Ritsema, J., van Heijst, H., 2000. Sci. Progress 83, 243-259.
30. Schubert, G., Turcotte, D.L., Olson, P., 2001. Cambridge Univ. Press, Cambridge etc, 940 pp.
31. Solomatov, V.S., 1995. Phys Fluids 7, 266-274.
32. Stacey, F.D., 1992. Physics of the Earth, 3rd edn., Brookfield Press, Brisbane, 513 pp.
33. Steinbach, V. , Yuen, D. A. , Zhao, W. L., 1993. Geophys. Res. Lett. 20, 1119 - 1122.
34. Steinbach, V., Yuen, D.A., 1994. Phys. Earth Planet. Inter. 86, 165-183.
35. Stevenson, D.J., Spohn, T., Schubert, G., 1983. Icarus 54, 466-489.
36. Tackley, P.J., 2000a. Geochem. Geophys. Geosyst., 1, Paper no. 2000GC000036.
37. Tackley, P.J., 2000b. Geochem. Geophys. Geosyst., 1, Paper no. 2000GC000043.
38. Trompert, R.A., Hansen, U., 1998. Nature 395, 686-689.
39. van der Hilst, R.D., Widiyantoro, S., Engdahl, E.R., 1997. Nature 386, 578-584.
40. Yang, W.-S., 1997. Thesis, Univ. of Illinois, Urbana-Champaign.
41. Zerr, A., Diegeler,A., Boehler, R., 1998. Science 281, 243-245.
42. Zhang, J., Herzberg, C., 1994. J. Geophys. Res. 99, 17729-17742.